RSC Advances

PAPER

View Article Online
View Journal | View Issue

Cite this: *RSC Adv.*, 2021, **11**, 15106

A biochar-promoted V_2O_5/g-C_3N_4 Z-Scheme heterostructure for enhanced simulated solar light-driven photocatalytic activity

Ya-Ni Zang, Shan-Shan Yang, * Jie Ding,* Shuang-Yang Zhao, Cheng-Xin Chen, Lei He and Nan-Qi Ren

A ternary biochar/vanadium pentoxide/graphite like carbon nitride (BC/V_2O_5/g-C_3N_4 denoted BC/VO/CN) composite was prepared by a simple hydrothermal method and its photocatalytic performance was investigated under simulated solar irradiation. The BC/VO/CN was characterized by X-ray diffraction, Fourier transform infrared spectroscopy, scanning electron microscopy, X-ray photoelectron spectroscopy, UV-vis diffuse reflectance spectroscopy, and photoluminescence spectroscopy. Within the BC/VO/CN composites VO nanoparticles were highly crystalline and intertwined with the lamellas of CN, resulting in the formation of well-defined Z-type heterostructures. The photocatalytic activity was evaluated using Rhodamine B as a model pollutant. Under simulated solar (230–780 nm) irradiation the as-prepared BC/VO/CN hybrid materials demonstrated highly improved photocatalytic activity compared to CN, VO and VO/CN. The cause of the solar enhancement could be ascribed to the formation of Z-type heterojunctions between VO and CN, which promoted faster electron–hole separation and more efficient charge transfer. BC, as an electron transfer medium, accelerated the transfer of photogenerated charge carriers and inhibited their recombination.

Received 7th April 2021
Accepted 8th April 2021

DOI: 10.1039/d1ra02712c

rsc.li/rsc-advances

1. Introduction

Semiconductor photocatalysis is an efficient and promising green technology that can utilize solar light energy to degrade organic or inorganic pollutants in wastewater treatment.[1,2] A number of traditional photocatalysts, such as titanium dioxide (TiO_2) and zinc oxide (ZnO) are only active in ultraviolet light, due to their large intrinsic band gap (3.0–3.2 eV). This results in an inefficient use of solar light or visible light (<5% of the solar spectrum) and, thus restricts their practical application.[3,4] Among the recently developed photocatalysts, graphitic carbon nitride (g-C_3N_4, denoted CN), a metal-free polymeric semiconductor material, is novel and increasingly important, due to its unique features: low cost, easy preparation, superior chemical properties, electron transfer capability, high thermal stability and optical properties.[5–8] And CN-based materials have been reported to diverse photocatalytic applications, such as photocatalytic hydrogen evolution,[9,10] photocatalytic CO_2 reduction,[11] and biomedical applications.[12] However, the photocatalytic performance of pure CN remains limited because deficient solar light absorption and the high recombination rate of photo induced electrons and holes leads to low quantum efficiency and photocatalytic activity.[13,14] Recent research on the fabrication of heterojunction photocatalysts, by coupling CN with other semiconductor materials or a metal and nonmetal, are considered one of the most effective methods to overcome the shortcomings of single component photocatalysts and effectively promote the separation of photogenerated carriers from recombination. However, the major disadvantage of the typical heterojunction photocatalytic system is that the photogenerated electrons and holes cannot maintain high reducibility and oxidation:[15] the reducibility of photogenerated electrons and the oxidizability of photogenerated holes weakens after the charge transfer.[16] Therefore, different methodologies are urgently required to prolong the electron–hole recombination process.

As a special kind of heterojunction, the construction of the Z-type heterojunction photocatalysis system is ideal and effective because it can reduce the recombination of photogenerated carriers and retain the photocatalytic redox ability.[17] Recently, some semiconductors with suitable band structures have been utilized to engineer CN-based direct Z-scheme systems, such as TiO_2/CN,[18] BiOCl/CN,[19] Bi_2O_3/CN[20] and WO_3/CN.[21] However, simply selecting semiconductors with band structures that are well-matched to CN can only contribute finitely to the development of CN-based Z-scheme photocatalysts.[22] For example, the band gaps of TiO_2 and BiOCl are large (>3.0 eV) and cannot respond to visible light. On the other hand, the response ranges of Bi_2O_3 and WO_3 are limited under visible light, with wavelengths <460 nm, which limits their solar energy conversion.

State Key Laboratory of Urban Water Resource and Environment, School of Environment, Harbin Institute of Technology, Harbin 150090, China. E-mail: shanshanyang@hit.edu.cn; dingjie123@hit.edu.cn

One of the disadvantages of the existing Z-type heterojunction system based on CN, is the inability to make full use of solar energy: enhancing visible-light absorption at the prerequisite efficient charge separation is a crucial factor when engineering carbon-nitride-based Z-scheme photocatalysts. Therefore, it is a major challenge to construct the CN-based direct solid-state Z-scheme system with a narrowband gap semiconductor photocatalyst for efficiently utilizing solar light.

Vanadium pentoxide (V_2O_5, denoted VO), which has chemical inertness, high oxidation ability and long-term stability against photochemical degradation, has been widely used in the preparation of various applications, such as catalysts, batteries and sensors[23–25] Furthermore, VO has a narrow band gap (2.3 eV), which directly responds to visible light and makes it a promising semiconductor photocatalyst for using solar energy. VO also has suitable band edges, which can match well with CN to form a direct solid-state Z-scheme photocatalytic system.[26] Recently, VO/CN composites have been widely used in the photocatalytic degradation of organic pollutants. Hong *et al.*[26] synthesized the Z-type VO/CN heterojunction photocatalysts by a facile *in situ* growth strategy, and the resulting photocatalyst is able to effectively degrade Rhodamine B (RhB). Sun *et al.*[27] prepared a series of VO-modified CN composites *via* a one-pot method, and demonstrated that the composite materials can make better use of visible light. Unfortunately, strategies focused on constructing the CN band structure for enhancing visible-light absorption in carbon-nitride-based Z-scheme systems are rarely reported. However, the transfer rate of photogenerated electrons is closely related to the photo catalytic efficiency of the Z-type heterojunction.

To improve the separation rate of photogenerated carriers, an electron transfer medium can be introduced. Some materials, such as reductive graphene oxide (rGO)[28] and graphene,[29] can be used as electron transfer media to accelerate the transfer of photogenerated electrons and enhance the separation of photogenerated carriers. However, the materials such as rGO and graphene are too expensive to be used on a large scale. Carbon materials, such as biochar (BC), have high electrical conductivity and are an excellent electron transfer medium, which can accelerate the transfer and separation of electrons. BC has strong mechanical properties and is easier to obtain than graphene oxide (GO) and other carbon materials. It has been widely used in electrochemical energy storage[30] as an adsorbent[31] and catalyst[32] carrier because of its good conductivity, rich functional groups and thermal stability.[33] Newly prepared BC can also have positive or negative net surface charges:[32] this improves its adsorptive effect on pollutants in water. BC doping can improve the stability of the photocatalyst, the adsorption capacity of pollutants and promote the separation of electrons and holes. However, to the best our knowledge, no studies have been conducted on using BC to promote VO/CN Z-Scheme heterostructure for enhanced simulated solar light-driven photocatalytic activity. In previous studies, BC is rarely mentioned as an electron transfer medium; therefore, it is necessary to study Z-type heterojunction system with BC.

In the present study, the VO/CN photocatalyst and BC modified Z-type heterojunction based VO/CN photocatalyst were synthesized by a simple hydrothermal method. In this study, RhB, which is a representative pollutant that harmful to human health and the surrounding environment,[34,35] was applied as a model organic pollutant to verify the photocatalytic performance of the synthesized ternary composite. The BC/VO/CN photocatalyst showed excellent catalytic performance for RhB degradation under simulated solar light. The results show that the properties of VO/CN are better than those of pure CN and VO and, compared to VO/CN, the photocatalytic rate of the ternary composite was improved. These results are due to the optical properties of CN and VO, the separation of photogenerated carriers in Z-type heterojunction system and the transfer of photogenerated electrons by BC as an electron transfer medium. The photocatalytic mechanism of the material was also analyzed. The results show that the ternary material has a certain application value.

2. Experimental

2.1. Materials

Reagents were all analytical grade and used without pretreatment, unless otherwise stated. Melamine, NH_4VO_3, ethylene diamine tetraacetic acid (EDTA), *p*-benzoquinone, isopropanol and RhB were purchased from Aladdin (China).

2.2. Photocatalyst synthesis

2.2.1. CN and VO. The synthesis of CN was done by the thermal treatment of melamine in a muffle furnace. Specifically, 10 g melamine was placed in a 50 mL alumina crucible, which was then calcined at a heating rate of 2.3 °C min^{-1} and maintained at 550 °C for 4 h. When the temperature dropped to 50 °C, the obtained samples were removed from the muffle furnace and left to cool. The obtained CN was collected and ground into a fine powder for subsequent analysis. Pure VO was also prepared by the thermal treatment in the muffle furnace. NH_4VO_3 (5.0 g) was put into a 50 mL alumina crucible and calcined at 500 °C for 1 h, at a heating rate of 5 °C min^{-1}. After being cooled to room temperature, the resulting products were collected and milled into VO powder in an agate mortar for further use.

2.2.2. VO/CN and BC/VO/CN composite photocatalyst. The VO/CN composite material was prepared by the simple hydrothermal method. Specifically, 0.6578 g of CN and different amounts of VO were added to deionized water in a flask. Polyvinylpyrrolidone (PVP) was simultaneously added as the dispersant and stirred for 1 h at room temperature. Then, the evenly stirred suspension was transferred into a stainless steel autoclave, lined with PVP and kept at 180 °C for 24 h. After cooling to room temperature, the resulting suspension was filtered, washed several times with deionized water and dried in an oven at 60 °C for 12 h. The dried product was ground into a fine powder in a mortar. The VO/CN composites, with VO mass fractions of 0.5%, 1.0%, 1.5%, 2.5% and 5.0% were labeled as 0.5% V, 1.0% V, 1.5% V, 2.5% V and 5.0% V, respectively.

The BC/VO/CN ternary material was fabricated in a similar way to the VO/CN binary material: pyrolysis of the as-prepared BC using rice straw was performed in a vacuum tube furnace (Vacuum tube furnace Shanghai Micro-X furnace Co., Ltd., Shanghai, China) under a nitrogen atmosphere (0.2 L min^{-1}) at 450 °C for 2 h. The pyrolysis heating rate was set at 15 °C min^{-1}. When the temperature dropped to room temperature, the pyrolyzed samples were removed from the furnace and transferred into 1 mol L^{-1} hydrochloric acid solution, followed by 24 h soaking. The samples were then filtered and washed several times, dried at 60 °C for 12 h and then ground to obtain the BC samples. For the synthesis of BC/VO/CN by the hydrothermal method, the as-prepared BC was doped using ultrasonic dispersion, before mixing with other monomers. The ternary composites doped with different mass fractions of BC were prepared and labeled as 1% BC, 5% BC and 15% BC, respectively. The fabrication of BC/VO and BC/CN binary composites was the same as the preparation process of BC/VO/CN ternary material, but without the addition of CN or VO. Before experiments, three times cleaning for all the as-prepared materials has been carried out. Fig. 1 illustrates the overall fabrication process of the BC/VO/CN composites.

2.3. Characterization

The surface morphology of the materials was analyzed by scanning electron microscope (SEM) on a Quanta 200 FEG SEM (SEM, FEI, American). The element composition and crystal structure of the materials were analyzed by X-ray diffraction (XRD) (D8 ADVANCE diffractometer, Bruker, Germany), with Cu Kα radiation ($k = 1.54056$) over the 2θ range of 5.0–80.0° at a scanning rate of 7.0° min^{-1}. FT-IR spectroscopy was performed on a Nicolet FT-IR spectrophotometer (Nexus 470, Thermo Electron Corporation) using KBr disks at room temperature. The atomic species and chemical states of the samples were analyzed by an X-ray photoelectron spectroscopy (XPS) electron spectrometer (Thermo Fisher ESCALAB 250Xi, America), using 150 W Al Kα X-ray sources. The ultraviolet-visible (UV-vis) diffused reflectance spectra (DRS) of the samples were achieved on an UV-vis spectrophotometer (UV-2550, Shimadzu, Japan), using $BaSO_4$ as a reflectance standard. The photoluminescence (PL) spectra of samples were measured on a HORIBA Scientific Fluoromax-4 at room temperature, using a fluorescence spectrophotometer (CHI 660B, Chenhua, China).

2.4. Photocatalytic activity experiments

The photocatalytic activity of the as-prepared photocatalyst samples was evaluated by the degradation of RhB under simulated solar irradiation. The degradation experiments were carried out in a 250 mL glass flask at room temperature. A xenon lamp used as a light source to simulated solar light was installed at a distance of 15 cm, providing an average power density of 300 mW cm^{-2} around the surface of the solution. Before photocatalysis, a certain amount of photocatalyst sample was added into 100 mL of 10 mg L^{-1} RhB solution and stirred for 30 min to achieve the adsorption–desorption equilibrium, in the dark. The concentration changes of RhB were evaluated at 554 nm (UV-2550 UV-vis spectrophotometer, Shimadzu, Japan) at 15 min intervals, using an UV-vis spectrophotometer of the suspensions. During the photocatalytic process, magnetic stirring was applied at a rotary speed of 480 rpm to ensure uniform dispersion of the photocatalyst particles, including CN, VO, VO/CN, BC/CN, BC/VO and BC/VO/CN, in the RhB solution. The suspension samples were immediately filtered through a 0.45 μm membrane to remove particulate. All experiments were performed in triplicate (average values ± standard deviation).

The effects of BC doping ratios were investigated. The degradation activity of the photocatalyst for RhB was

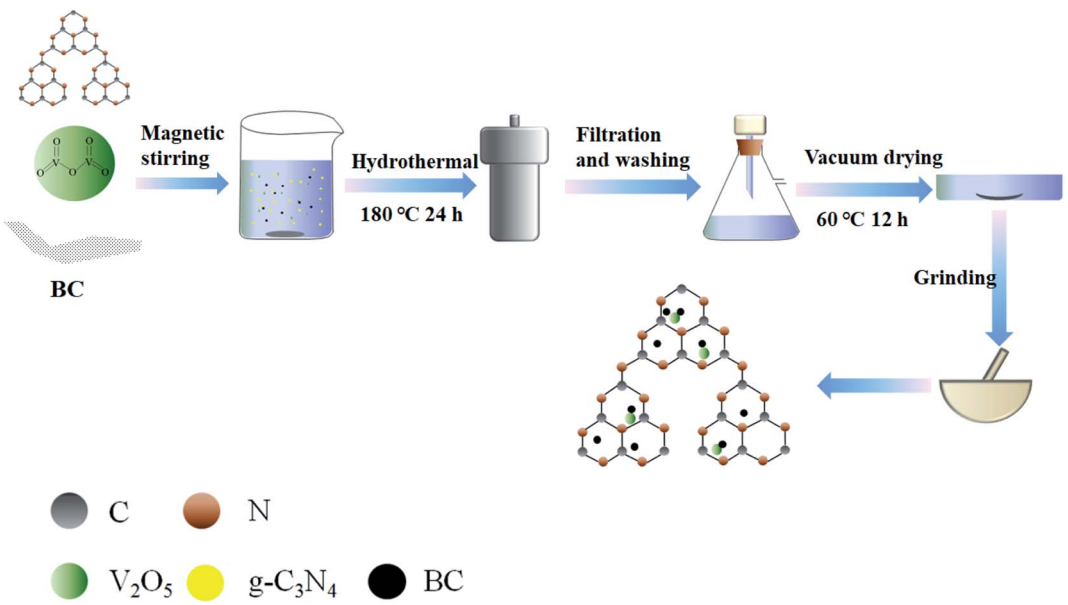

Fig. 1 Fabrication process of the BC/VO/CN composite.

investigated when the doping ratios of BC were 1%, 5% and 15%, and the doping amount of BC was optimized.

Recycling tests were performed to measure the stability of catalysts under solar light irradiation. After each cycle of the photocatalytic reaction, the sample was separated from the reaction mixture by centrifugation, washed several times with double distilled water and dried overnight in the vacuum drying oven at 60 °C for use in the next cycle. The recycling experiments were repeated 5 times.

2.5. Active species trapping experiments

To determine the reaction mechanism, quenching experiments were carried out to identify the active substances crucial to photocatalysis. *p*-Benzoquinone,[26] isopropanol[26] and EDTA[36] (3 mM) were added to the RhB solution (100 mL, 10 mg L^{-1}) to capture the superoxide radical ($^{\bullet}O_2^-$), h^+ and hydroxyl radical ($^{\bullet}OH$). In addition, the electron spin resonance (ESR) technique was used to detect the presence of $^{\bullet}OH$ and $^{\bullet}O_2^-$ radicals in the photocatalytic reaction system under simulated solar light ($320 < \lambda < 780$ nm). The $^{\bullet}OH$ and $^{\bullet}O_2^-$ radicals can be trapped by 5,5-dimethyl-1-pyrroline *N*-oxide (DMPO).[28] Before determining the hydroxyl radicals (DMPO-$^{\bullet}OH$) and superoxide radicals (DMPO-$^{\bullet}O_2^-$), 10.0 mg of sample was dissolved in 0.5 mL deionized water (DMPO-$^{\bullet}OH$) or 0.5 mL methanol (DMPO-$^{\bullet}O_2^-$). Then, 45 μL DMPO was added and dispersed through ultrasonication for 5 min. All experiments were performed in triplicate (average values ± standard deviations).

3. Results and discussion

3.1. Textural characterization

Crystalline phases of the as-prepared samples were determined by XRD analysis. As shown in Fig. 2a, the diffraction peaks of pure CN were observed at 13.099° and 27.620°, which could be attributed to the (100) and (002) diffraction planes of graphite-like carbon nitride, respectively. They also correspond to the periodic arrangement of heptazine (that is, the basic structural unit in the CN layer) and the typical stacking peaks of aromatic rings. Based on the results CN could be successfully prepared by heat treatment with sufficient crystallinity and high purity. The diffraction peak of pure VO was compared with the JCPDS 41-1426 standard card, and it was ascertained that the prepared sample was orthorhombic. Therefore, it was found that fully crystalline and relatively pure VO could be prepared by heat treatment using ammonium metavanadate as precursor. For bare BC, a broad diffraction peak was observed at about 27.396°, which can be ascribed to the reflection of the (008) crystallographic plane. For the binary VO/CN and ternary BC/VO/CN systems, no diffraction peaks of VO and BC were found, which might be due to the weak diffraction intensities or their low content.

To further confirm the presence of VO and BC in the ternary samples, FT-IR measurements were carried out. As shown in Fig. 2b, the band at 809 cm^{-1} could be attributed to *s*-triazine rings. The bands at 1236, 1320, 1405, 1547, and 1634 cm^{-1} with high intensities correspond to the stretching vibration modes of C=N and aromatic C–N heterocycles. For VO two characteristic absorption bands were observed at 829 cm^{-1} and 1018 cm^{-1}. The former could be attributed to the asymmetric stretching modes of V–O–V bonds while the latter to the stretching vibration of V=O bonds. As expected, the FT-IR spectrum of VO/CN was the combination of that of CN and VO. Similarly, the FT-IR spectrum of BC/VO/CN was the combination of the FT-IR spectra of CN, VO and BC, and no impurities were detected.

The chemical state and surface chemical composition of BC (5%)/VO (1.5%)/CN were examined by XPS. As show in Fig. 3 in the C 1s spectrum, the peaks at 281.8 eV and 284.9 eV could be assigned to the N–C–N coordination in CN. In the N 1s spectra, the main N 1s peak at 395.6 eV was attributed to sp^2-hybridized nitrogen (C=N–C). In the V 2p spectrum the peaks at 514.4 eV and 521.8 eV were ascribed to V $2p_{3/2}$ and V $2p_{1/2}$ levels, while the peak at 529.4 eV in the O 1s spectrum corresponds to the oxygen atom of VO.

The morphology of the samples was investigated by SEM (Fig. 4). The shape of CN was irregular, including massive, spherical, flocculent structures. VO is a hard block structure with folds and stacking inside. In the VO/CN sample, the spherical solid increased and the massive structure was compounded on the spherical structure. The BC was columnar with

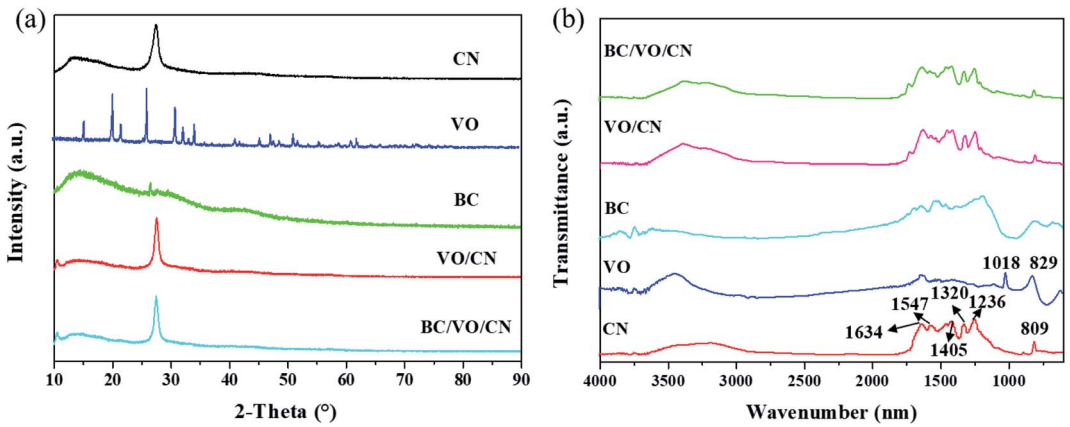

Fig. 2 (a) XRD patterns of as-prepared photocatalysts; (b) FT-IR spectra of as-prepared photocatalysts.

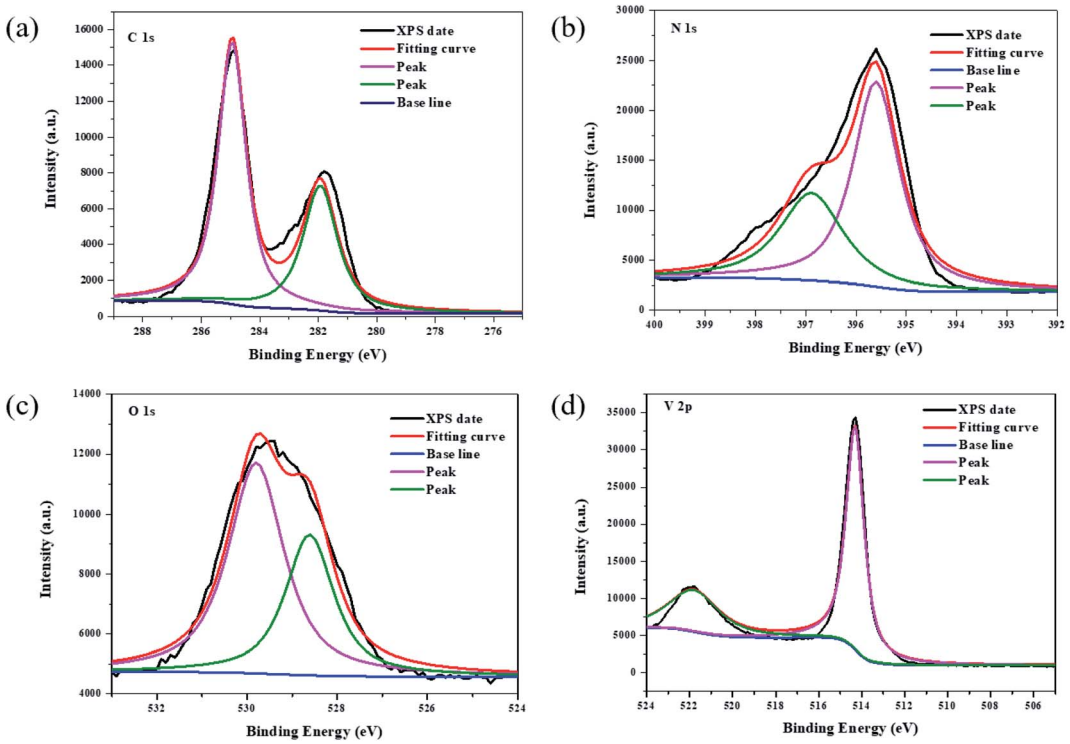

Fig. 3 XPS spectra of BC/VO/CN sample (a) C 1s; (b) N 1s; (c) O 1s; and (d) V 2p.

regular pattern. The SEM images of the ternary sample showed that CN and VO were successfully loaded on BC. Moreover, the energy dispersive X-ray spectrometer (EDS) (Fig. 5) also reinforced that these materials were successfully combined.

The UV-vis diffuse reflectance spectra were shown in Fig. 6a. Pure CN showed absorptions both in the ultraviolet and visible light regions up to 480 nm, while bare VO exhibited a sharp absorption edge at about 610 nm. Compared with that of pure CN, the absorption edges of the BC (1%)/VO (1.5%)/CN, BC (5%)/VO (1.5%)/CN and BC (15%)/VO (1.5%)/CN have showed a redshift. Moreover, the more BC doping, the greater the red shift. The results imply that all of the photocatalysts could absorb visible light. The band gap energy (E_g) of the samples were calculated based on the following formula:

$$\alpha h\nu = A(h\nu - E_g)^{n/2} \quad (1)$$

where α, h, ν, A and E_g represent the absorption coefficient, Planck constant, light frequency, proportionality constant, and band gap energy, respectively. As shown in Fig. 6b, the band gaps of CN and VO were calculated to be 2.75 eV and 2.17 eV, respectively, which are nearly identical to the values from previous publications. For VO/CN, BC (1%)/VO (1.5%)/CN, BC (5%)/VO (1.5%)/CN and BC (15%)/VO (1.5%)/CN, the band gaps energies were found to be 2.77, 2.73, 2.60 and 2.37 eV, respectively. In the experiment, the narrower the band gap is, the easier the photogenerated electron transfer to the conduction band. Therefore, according to Fig. 6, the electron transition of 15% BC is most likely to occur. However, the narrower the band gap is, the easier the photogenerated carriers are to recombine. The large amount of BC of 15% BC affects the absorption and reflection of UV and visible light, which leads to abnormal phenomenon of RhB degradation. In addition, with the increase of BC doping, the band gap becomes narrower and narrower, which may be due to the band gap mixing effect of the two and the interaction of the two semiconductors at the interface, thereby introducing the level of defects[37] or the increase in BC content and the accompanying increase in function groups affecting the crystalline morphology of g-C_3N_4 and V_2O_5.[38]

PL analysis was carried out to investigate the separation and the transfer ability of photoinduced charge carriers. To measure the PL emission spectra of the samples 350 nm was set as excitation wavelength. It is well-known that higher PL intensity indicates faster recombination of charge carriers, resulting in lower photocatalytic activity. As shown in Fig. 7, VO/CN had a main emission peak at about 460 nm, which corresponds to its band gap and could be ascribed to the recombination of electron–hole pairs. After the BC was introduced, the samples showed lower PL emission intensity compared with that of VO/CN, suggesting that the recombination rate of photogenerated charge carriers decreased in BC/VO/CN. Therefore, the introduction of BC could accelerate the transfer rate of photogenerated electrons and inhibit the recombination of photogenerated charge carriers. PL results showed that the more BC doping, the better the photogenerated carrier separation. However, in practical application, because the color of BC is black, excessive doping of BC will cause poor absorption of light in solution. Thus, the PL results were inconsistent with the

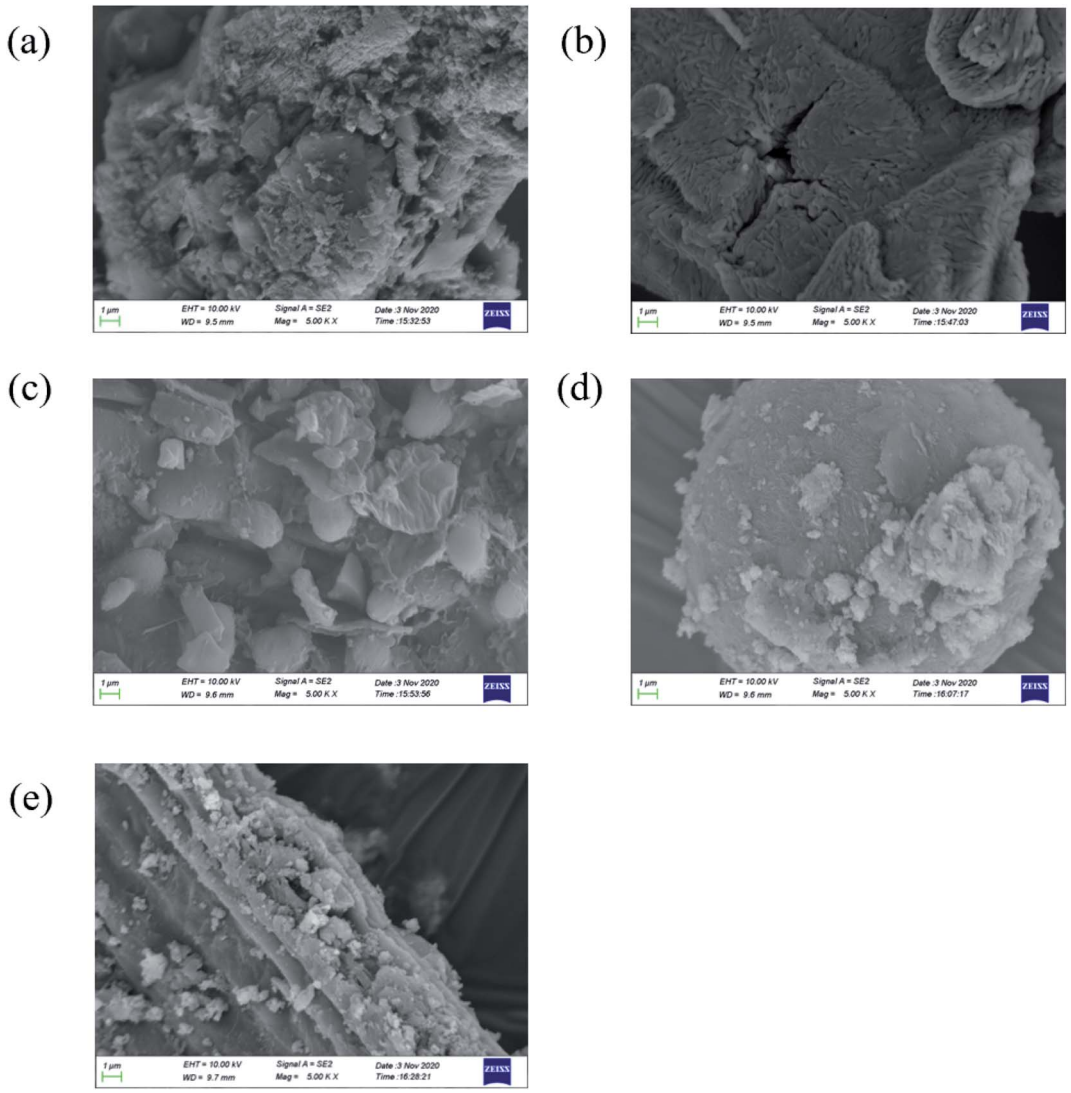

Fig. 4 SEM of (a) CN; (b) VO; (c) BC; (d) VO (1.5%)/CN; (e) BC (5%)/VO (1.5%)/CN.

degradation effect of RhB by dosing 15%BC. Similar observations have been obtained in previous studies.[27]

3.2. Photocatalytic activity

The photocatalytic activities of the as-prepared samples were evaluated by the degradation of RhB as a model pollutant under simulated solar light (320 nm < λ < 780 nm). As shown in Fig. 8a, RhB does not decompose in the absence of light and catalyst. The test without the catalyst reveals that the photolysis of RhB occurs very slowly, which can be negligible. Pure CN (62%) and raw VO (56%) have a poor degradation effect on RhB under simulated solar light. However, the as-prepared VO/CN heterojunction photocatalysts can efficiently enhance the photocatalytic activity, compared to individual CN and VO, when the mass fraction of doped VO is 1.5%. Based on the preparation of binary materials, BC was doped, which improved the degradation of RhB. The influence of BC doping ratio on RhB shows that with the increase of BC doping mass fraction, the adsorption capacity of ternary materials for RhB increased, and the degradation effect of ternary materials was better than that of binary materials. When the mass fraction of BC is 5%, the degradation e of RhB reaches its highest efficiency (99.7%) within 60 min. To further prove the photocatalytic ability of the ternary composites, the prepared BC/CN and BC/VO doped with 5 wt% BC were used to degrade RhB. The results showed that the ternary photocatalyst with 5 wt% BC doping had the best degradation ability on RhB.

The kinetic behaviors of as-prepared samples for photodegradation of RhB were investigated further. As illustrated in Fig. 8b, all of them fit well with the pseudo-first order correlation:

$$\ln \frac{C_0}{C} = kt \quad (2)$$

where C is the concentration of RhB remaining in the solution at irradiation time of t. C_0 is the initial concentration at $t = 0$, and k is the degradation apparent rate constant. The k values of

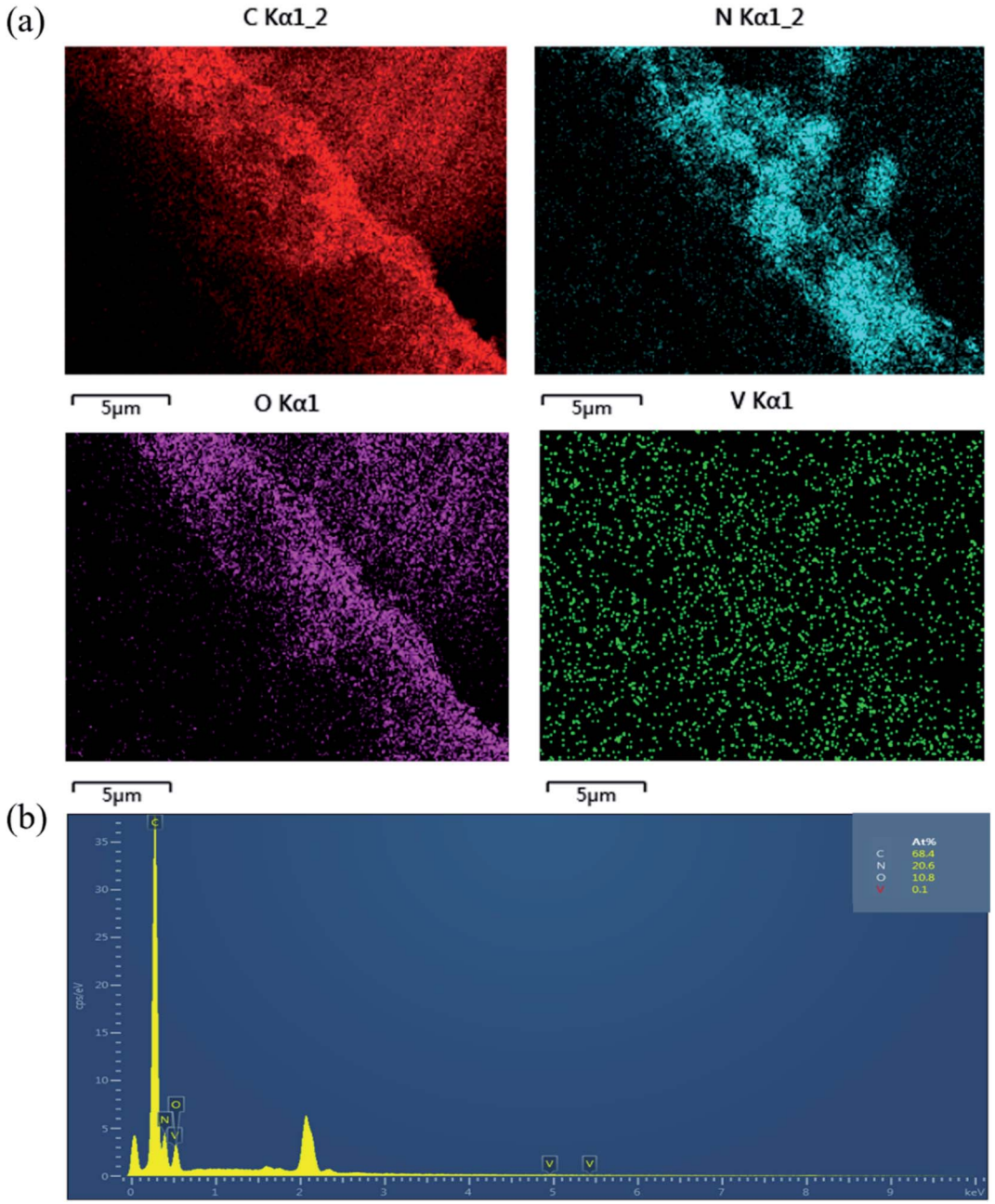

Fig. 5 (a) Element distribution of BC (5%)/VO (1.5%)/CN; (b) EDS of BC (5%)/VO (1.5%)/CN.

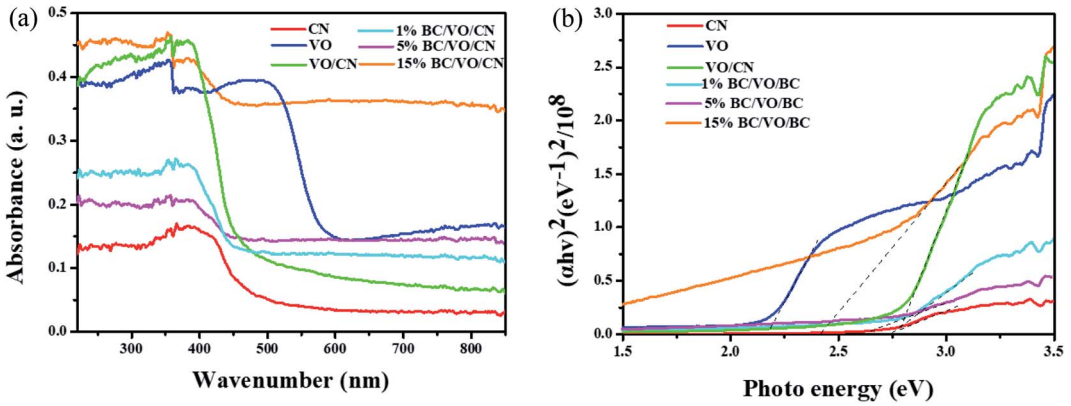

Fig. 6 (a) UV-vis absorption spectra of as-prepared samples; (b) $(\alpha h\nu)^2$–$h\nu$ curves of as-prepared samples.

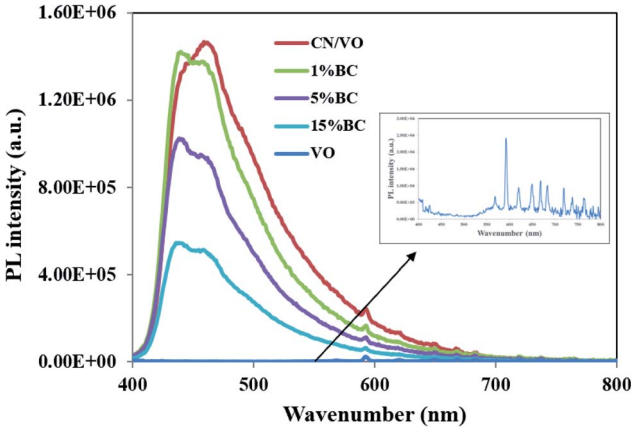

Fig. 7 PL emission spectra for as-prepared samples.

different samples are shown in Table 1: under the same experimental conditions, the kinetic constant of RhB degradation over BC/VO/CN can reach 0.056 min^{-1}, which was significantly higher than those of single-component CN (0.0154 min^{-1}) and VO (0.0129 min^{-1}), as well as binary VO/CN (0.0386 min^{-1}).

From Fig. 8c, it can be observed that the photocatalytic activity of BC/VO/CN with 5 wt% BC has no apparent deactivation (96.5%), even after five successive recycles for RhB degradation under simulated solar light irradiation. This demonstrates that our photocatalyst possesses high stability in practical applications. Furthermore, the XRD pattern of the BC/VO/CN with 5 wt% BC after the fifth run cycle was determined (Fig. 8d), and it can be clearly observed that the phase and structure of the BC/VO/CN with 5 wt% BC remained unchanged. This suggests that the sample remains stable, even after the fifth run cycle in the photocatalytic degradation processes.

Based on the results obtained in this study, the RhB degradation capacities by different photocatalytic reaction were further compared in terms of catalytic performances using various catalysts (such as vanadium oxide/activated carbon, Ni-doped VO, $Na_2Ti_3O_7$ nanotube-VO, 1D Ag/AgCl/VO, *etc.*), as reported in literature studies (Table 2). Moreover, the composite of VO and other materials can enhance the effect of photocatalytic degradation of RhB. Therefore, VO is an excellent semiconductor material which can be used to make photocatalyst. In this study, the doping of CN forms a Z-scheme heterojunction system, and the doping of BC makes the

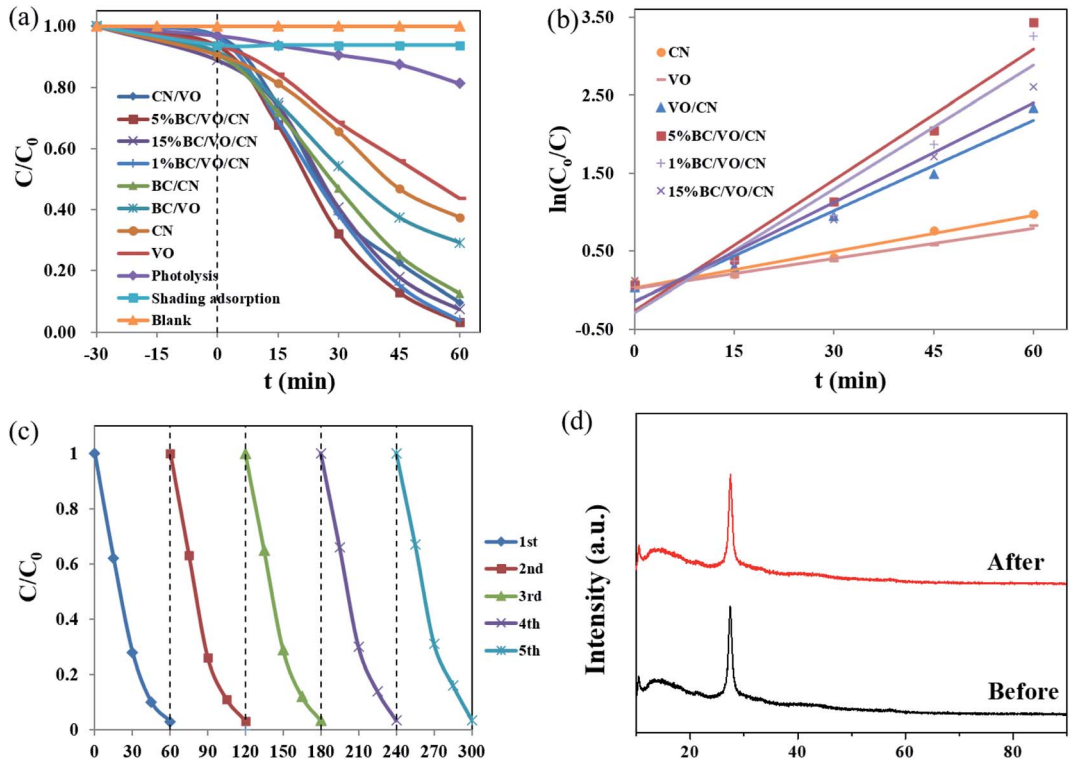

Fig. 8 (a) The photocatalytic activities of as-prepared samples for RhB degradation. (b) The pseudo-first-order reaction kinetics for RhB degradation. (c) Cycling runs of BC (5%)/VO (1.5%)/CN photocatalyst under simulated solar light irradiation. (d) The XRD patterns of BC (5%)/VO (1.5%)/C_3N_4 before and after five recycling runs.

Table 1 The pseudo-first order constants for RhB degradation under simulated solar light irradiation

Samples	5% BC/VO/CN	1% BC/VO/CN	15% BC/VO/CN	VO/CN	CN	VO
k (min^{-1})	0.056	0.0529	0.0426	0.0386	0.0154	0.0129

Table 2 Comparison of properties of different materials for photocatalytic degradation of RhB

Catalyst	Irradiation condition	RhB	Catalytic performance	Reference
BC/V_2O_5/g-C_3N_4	60 min under simulated solar light	100 mL of 10 mg L^{-1}	99.7% removal	—
Ni-doped V_2O_5	20 min under visible light irradiation	100 ppm	98% removal	39
Vanadium oxide/activated carbon	5 h under visible light irradiation	200 mL of 10 mg L^{-1}	89.4% removal	40
$Na_2Ti_3O_7$ nanotube-V_2O_5	80 min under visible light irradiation	100 mL of 5 ppm in concentration	97.4% removal	41
PANI/$V_2O_5 \cdot nH_2O$ heterojunction	300 min under visible light irradiation	100 mg of 5 mg L^{-1}	79.5% removal	42
1D Ag/AgCl/V_2O_5	180 min under visible light irradiation	50 mL of 10 mg L^{-1}	93.8% removal	43
Zn doped V_2O_5	30 min of solar light irradiation	—	45% removal	44
Surface fluorinated bismuth vanadate crystals	360 min of visible light irradiation	20 mL of 1 × 10^{-5} mol L^{-1}	>90% removal	45
TiO_2@SiO_2/Ag nanocomposites	Under direct sunlight	—	92% removal	46
$Cu_{2-x}Se$ nanoplates	120 min of visible light irradiation	50 mg of 10 mg L^{-1}	50% removal	47

electron efficiency higher, which further improves the photocatalytic degradation of RhB. By comparison, it is found that BC has stronger photocatalytic than photocatalysts of the existing researches.

3.3. Photocatalytic mechanism

The mechanism of the photocatalytic degradation was investigated by quenching experiments. 3 mmol L^{-1} isopropanol, *p*-benzoquinone and EDTA were added to 100 mL solution of 10 mg L^{-1} to capture $^{\cdot}OH$, $^{\cdot}O_2^-$, and h^+ in the solution respectively. There are several reactions that may produce active substances in photocatalytic reaction.

$$e^- + O_2 \rightarrow {}^{\cdot}O_2^- \quad (3)$$

$${}^{\cdot}O_2^- + e^- + 2H^+ \rightarrow H_2O_2 \quad (4)$$

$${}^{\cdot}O_2^- + H_2O \rightarrow {}^{\cdot}OH + OH^- + O_2 \quad (5)$$

$$H_2O_2 \rightarrow 2{}^{\cdot}OH \quad (6)$$

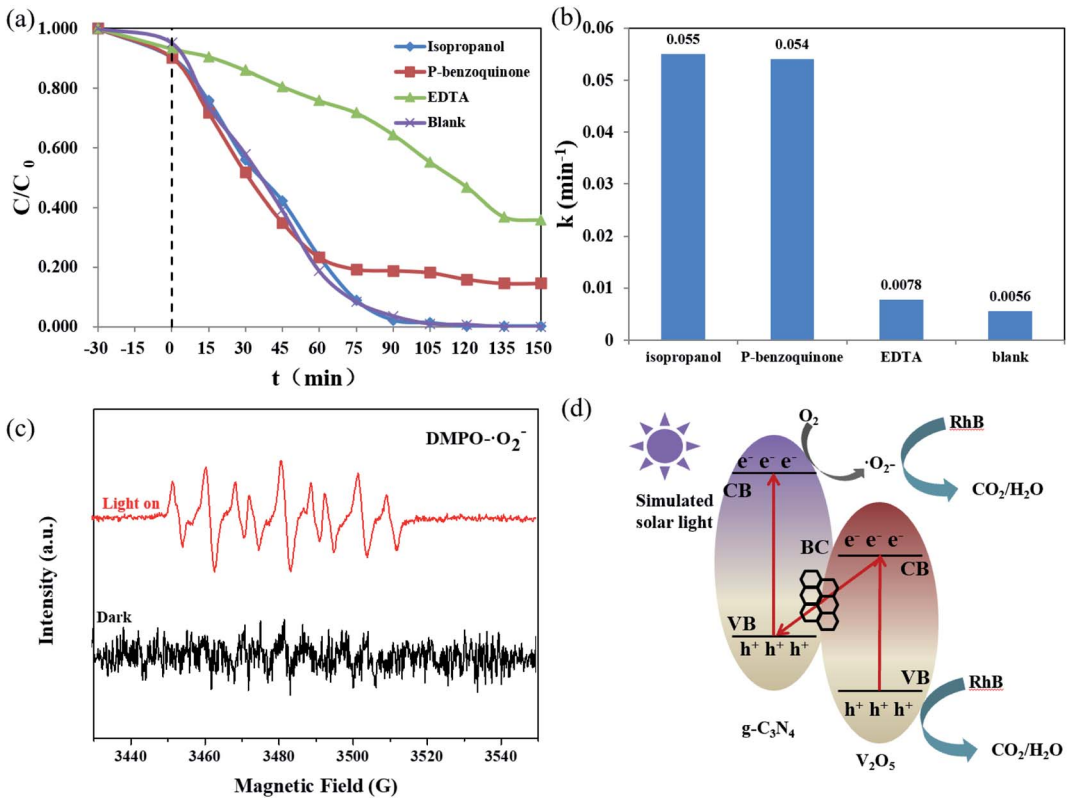

Fig. 9 (a) The species trapping experiments for degradation of RhB over BC (5%)/VO (1.5%)/CN photocatalysts under simulated solar light irradiation. (b) The *k* values of the species trapping experiments. (c) DMPO spin-trapping ESR spectra in aqueous dispersion of BC (5%)/VO (1.5%)/CN for DMPO-$^{\cdot}O_2^-$. (d) The possible photocatalytic mechanism of BC (5%)/VO (1.5%)/CN heterojunction photocatalysts for degradation of organic pollutants under simulated solar light irradiation.

It can be seen from Fig. 9a that the addition of EDTA and *p*-benzoquinone in habited the degradation of RhB under simulated sunlight, while the addition of isopropanol had little effect on the degradation of RhB. Fig. 9b is the kinetic constant obtained by calculation when different capture agents are added. It can be found that the addition of EDTA and *p*-benzoquinone significantly reduces the reaction kinetic constant of RhB. In short, the results showed that the contribution of $^{\bullet}OH$ to the photocatalytic reaction was very small, while $^{\bullet}O_2^-$ and h^+ played a major role in it. In general, photogenerated electrons can reduce oxygen molecules to superoxide anions, which can react with RhB molecules and degrade them to CO_2 and H_2O. At the same time, photogenerated holes can react directly with RhB molecules. To further explore the reaction mechanism, the band edges of CN and VO were calculated. For the calculations the following formula was applied:

$$E_{CB} = X - E^e - \frac{1}{2}E_g \quad (7)$$

$$E_{VB} = E_{CB} + E_g \quad (8)$$

where the X for CN and VO are 4.73 and 6.10 eV, respectively. E^e is the energy of free electrons on the hydrogen scale ($E^e = 4.5$ eV), and E_g is the band gap energy of the semiconductor (which was 2.75 eV for CN and 2.17 eV for VO). The E_{CB} and E_{VB} of CN were −1.15 eV and 1.60 eV, respectively, while they were 0.52 eV and 2.69 eV for VO, respectively. For CN, the potential of the conduction band was more negative than that of $O_2/^{\bullet}O_2^-$ (−0.33 eV), so O_2 could react with the conduction band electrons of CN to form $^{\bullet}O_2^-$. However, the valence band potential of CN was lower than that of $^{\bullet}OH$, H^+/H_2O (2.72 eV), so the valence band holes of CN could not oxidize H_2O to $^{\bullet}OH$. For VO, the potential of the conduction band was less negative than that of $O_2/^{\bullet}O_2^-$ (−0.33 eV), thus the photogenerated electrons in the conduction band could not react with O_2 to form $^{\bullet}O_2^-$. The redox potential of VO was lower than that of $^{\bullet}OH$, H^+/H_2O (2.72 eV), and the valence band holes of VO could not react with H_2O to form $^{\bullet}OH$.

ESR measurements were carried out to further investigate the formation of $^{\bullet}OH$ and $^{\bullet}O_2^-$ radicals in BC (5%)/VO (1.5%)/CN under simulated solar irradiation solar. As shown in Fig. 9c, no ESR signal corresponding to the DMPO-$^{\bullet}O_2^-$ adduct was found for BC (5%)/VO (1.5%)/CN in the dark, indicating that no detectable $^{\bullet}O_2^-$ species were formed as expected. However, when the light was turned on, a strong ESR signal was observed due to the formation of $^{\bullet}O_2^-$ radicals. However, the signal of $^{\bullet}OH$ was not found in the whole process.

Based on the results mentioned above, a novel Z-scheme mechanism (Fig. 9d) was proposed to explain the cause of the enhanced photocatalytic activity of the VO/CN heterojunctions. CN and VO can produce photogenerated electron–hole pairs under simulated solar light irradiation. If the migration path of photogenerated electrons follows the way of a typical heterojunction system, the conduction band electrons in VO will produce a very few numbers of $^{\bullet}O_2^-$ radicals because of their low reducibility. This is inconsistent with the experimental results. The conduction band electrons in VO tend to combine with the valence band holes in CN. At the same time, the number of conduction band electrons in CN gradually increase, then they react with O_2 to form a large number of $^{\bullet}O_2^-$ radicals. These radicals are strongly oxidative, and can degrade RhB molecules to CO_2 and H_2O. At the same time, the photogenerated holes in the valence band of VO can react directly with the RhB molecules and oxidize them to CO_2 and H_2O.

Combining the results of PL and UV-vis DRS measurements, it was found that BC acted as an electron transfer medium, promoting the transfer and separation of photogenerated charge carriers. Therefore, BC (5%)/VO (1.5%)/CN followed the electron transfer rule of Z-type heterojunction systems, improving the separation and transfer of photogenerated charge carriers, enhancing the efficiency of RhB degradation.

4. Conclusions

The ternary BC (5%)-promoted VO/CN Z-scheme heterostructures were synthesized by a simple hydrothermal method, which showed excellent photocatalytic performance for RhB degradation under simulated solar irradiation. BC/VO/CN composite degraded RhB with 3.64-, 4.34-, and 1.45-times higher efficiency compared to CN, VO, and VO/CN, respectively. The existence of a Z-scheme heterojunction promoted the effective separation of photogenerated electrons and holes. The introduction of BC accelerated the electron migration rate. The ternary photocatalyst had good stability and could be recycled. This study shows that the as-prepared BC (5%)/VO (1.5%)/CN ternary photocatalyst have application value and prospect in the degradation of organic pollutants.

Conflicts of interest

The authors declare that they have no known competing financial interests or personal relationships that could have appeared to influence the work reported in this paper.

Acknowledgements

This work was supported by the National Nature Science Foundation of China (Grant No. 51778175); the State Key Laboratory of Urban Water Resource and Environment (Harbin Institute of Technology) [Grant No. 2021TS03].

References

1 J. F. Leal, S. M. A. Cruz, B. T. A. Almeida and V. L. Esteves, TiO_2-rGO nanocomposite as an efficient catalyst to photodegrade formalin in aquaculture's waters, under solar light, *Environ. Sci.: Water Res. Technol.*, 2020, **6**, 1018–1027.

2 C. Singh, R. Chaudhary and K. Gandhi, Solar photocatalytic oxidation and disinfection of municipal wastewater using advanced oxidation processes based on pH, catalyst dose, and oxidant, *J. Renewable Sustainable Energy*, 2013, **5**, 51–57.

3 S. A. Bilmes, P. Mandelbaum, F. Alvarez and N. M. Victoria, Surface and Electronic Structure of Titanium Dioxide Photocatalysts, *J. Phys. Chem. B*, 2000, **104**, 9851–9858.
4 P. R. Potti and V. C. Srivastava, Effect of Dopants on ZnO Mediated Photocatalysis of Dye Bearing Wastewater: A Review, *Mater. Sci. Forum*, 2013, **757**, 165–174.
5 S. C. Yan, Z. S. Li and Z. G. Zou, Photodegradation Performance of g-C_3N_4 Fabricated by Directly Heating Melamine, *Langmuir*, 2009, **25**, 10397–10401.
6 J. Yu, S. Wang, J. Low and W. Xiao, Enhanced photocatalytic performance of direct Z-scheme g-C_3N_4-TiO_2 photocatalysts for the decomposition of formaldehyde in air, *Phys. Chem. Chem. Phys.*, 2013, **15**, 16883–16890.
7 F. Chang, J. Zhang, Y. Xie, J. Chen, C. Li, J. Wang, J. Luo, B. Deng and X. Hu, Fabrication, characterization, and photocatalytic performance of exfoliated g-C_3N_4-TiO_2 hybrids, *Appl. Surf. Sci.*, 2014, **311**, 574–581.
8 B. Zhu, P. Xia, W. Ho and J. Yu, Isoelectric point and adsorption activity of porous g-C_3N_4, *Appl. Surf. Sci.*, 2015, **334**, 188–195.
9 G. F. Liao, Y. Gong, L. Zhang, H. Y. Gao, G. J. Yang and B. Z. Fang, Semiconductor polymeric graphitic carbon nitride photocatalysts: the "holy grail" for photocatalytic hydrogen evolution reaction under visible light, *Energy Environ. Sci.*, 2019, **12**, 2080–2147.
10 Y. Liu, S. Shen, Z. Li, D. Ma, G. Xu and B. Fang, Mesoporous g-C_3N_4 nanosheets with improved photocatalytic performance for hydrogen evolution, *Mater. Charact.*, 2021, **174**, 111031.
11 G. F. Liao, C. X. Li, X. Z. Li and B. Z. Feng, Emerging polymeric carbon nitride Z-scheme systems for photocatalysis, *Cell Rep. Phys. Sci.*, 2021, **2**, 100355.
12 G. F. Liao, F. He, Q. Li, L. Zhong, R. Z. Zhao, H. N. Che, H. Y. Gao and B. Z. Fang, Emerging graphitic carbon nitride-based materials for biomedical applications, *Prog. Mater. Sci.*, 2020, **112**, 100666.
13 Q. Wang, S. Xu and F. Shen, Preparation and characterization of TiO_2 photocatalysts co-doped with iron (III) and lanthanum for the degradation of organic pollutants, *Appl. Surf. Sci.*, 2011, **257**, 7671–7677.
14 A. Kumar, M. Khan, L. P. Fang and I. M. C. Lo, Visible-light-driven N-TiO_2@SiO_2@Fe_3O_4 magnetic nanophotocatalysts: synthesis, characterization, and photocatalytic degradation of PPCPs, *J. Hazard. Mater.*, 2017, **370**, 108–116.
15 S. Hu, F. Zhou, L. Wang and J. Zhang, Preparation of Cu_2O/CeO_2 heterojunction photocatalyst for the degradation of Acid Orange 7 under visible light irradiation, *Catal. Commun.*, 2011, **12**, 794–797.
16 D. Wang, H. Shen, G. Li, F. Fu and Y. Liang, Design and construction of the sandwich-like Z-scheme multicomponent CdS/Ag/Bi_2MoO_6 heterostructure with enhanced photocatalytic performance in RhB photodegradation, *New J. Chem.*, 2016, **10**, 1039.
17 J. Zhang, Y. Hu, X. Jiang, S. Chen and S. Meng, Design of a direct Z-scheme photocatalyst: preparation and characterization of Bi_2O_3/g-C_3N_4 with high visible light activity, *J. Hazard. Mater.*, 2014, **280**, 713–722.
18 T. S. Natarajan and W. K. Jo, Influence of TiO_2 morphology on the photocatalytic efficiency of direct Z-scheme g-C_3N_4/TiO_2 photocatalysts for isoniazid degradation, *Chem. Eng. J.*, 2015, **283**, 549–565.
19 Y. Bai, P. Q. Wang, J. Y. Liu and X. J. Liu, Enhanced photocatalytic performance of direct Z-scheme BiOCl–g-C_3N_4 photocatalysts, *RSC Adv.*, 2014, **4**, 19456–19461.
20 J. Zhang, H. Qian, W. Liu, H. Chen, Y. Qu and Z. Lin, The Construction of the Heterostructural Bi_2O_3/g-C_3N_4 Composites with an Enhanced Photocatalytic Activity, *Nano*, 2018, **13**, 55–63.
21 H. Katsumata, Y. Tachi and T. Suzuki, Z-scheme photocatalytic hydrogen production over WO_3/g-C_3N_4 composite photocatalysts, *RSC Adv.*, 2014, **4**, 21405–21409.
22 J. Fu, J. Yu, C. Jiang and B. Cheng, g-C_3N_4 based Heterostructured Photocatalysts, *Adv. Eng. Mater.*, 2018, **8**, 1701503.
23 A. D. Raj, T. Pazhanivel, P. S. Kumar, D. Mangalaraj and N. Ponpandian, Self assembled V_2O_5 nanorods for gas sensors, *Curr. Appl. Phys.*, 2010, **10**, 531–537.
24 A. Z. Moshfegh and Z. Lgnatiev, Photo-enhanced catalytic decomposition of isopropanol on V_2O_5, *Catal. Lett.*, 1990, **4**, 113–122.
25 B. Li, Y. Xu, G. Rong, M. Jiang and Y. Xie, Vanadium pentoxide nanobelts and nanorolls: from controllable synthesis to investigation of their electrochemical properties and photocatalytic activities, *Nanotechnology*, 2006, **17**, 2560–2566.
26 Y. Hong, Y. Jiang, C. Li, W. Fan, X. Yan and M. Yan, In-situ synthesis of direct solid-state Z-scheme V_2O_5/g-C_3N_4 heterojunctions with enhanced visible light efficiency in photocatalytic degradation of pollutants, *Appl. Catal., B*, 2018, 663–673.
27 X. Sun, C. Fan, X. Cheng, Q. Liu and H. Tang, One-pot synthesis of g-C_3N_4/V_2O_5 composites for visible light-driven photocatalytic activity, *Appl. Surf. Sci.*, 2015, **358**, 188–195.
28 D. Jiang, P. Xiao, L. Shao, D. Li and M. Chen, RGO-Promoted All-Solid-State g-C_3N_4/$BiVO_4$ Z-Scheme Heterostructure with Enhanced Photocatalytic Activity toward the Degradation of Antibiotics, *Ind. Eng. Chem. Res.*, 2017, **56**, 8823–8832.
29 X. H. Li, J. S. Chen, X. C. Wang, J. H. Sun and M. Antonietti, Metal-free activation of dioxygen by graphene/g-C_3N_4 nanocomposites: functional dyads for selective oxidation of saturated hydrocarbons, *J. Am. Chem. Soc.*, 2011, **133**(21), 8074–8077.
30 B. H. Cheng, R. J. Zeng and H. Jiang, Recent developments of post-modification of biochar for electrochemical energy storage, *Bioresour. Technol.*, 2017, **246**, 224–233.
31 X. F. Tan, Y. G. Liu, Y. L. Gu, Y. Xu and J. Li, Biochar-based nano-composites for the decontamination of wastewater: a review, *Bioresour. Technol.*, 2016, **212**, 318–333.
32 J. Lee, K. H. Kim and E. E. Kwon, Biochar as a Catalyst, *Renewable Sustainable Energy Rev.*, 2017, **77**, 70–79.
33 B. T. Nguyen, J. Lehmann, W. C. Hockaday and S. Joseph, Temperature Sensitivity of Black Carbon Decomposition and Oxidation, *Environ. Sci. Technol.*, 2010, **44**, 3324.

34 L. L. Bao, M. J. Meng, K. Y. Sun, W. B. Li and D. X. Zhao, Selective adsorption and degradation of rhodamine B with modified titanium dioxide photocatalyst, *J. Appl. Polym. Sci.*, 2014, **131**(20), 40890.

35 H. Yang, E. Li, B. Zhou, Y. Wang and S. Xia, Preparation and Characterization of a g-C_3N_4/LSACF Composite and Application in RhB Degradation, *J. Inorg. Organomet. Polym. Mater.*, 2019, **30**(4), 1463–1472.

36 K. Geng, Y. Wu, G. D. Jiang, K. L. Liu and L. L. Jiang, RuC@g-C_3N_4 (H^+)/TiO_2 visible active photocatalyst: facile fabrication and Z-scheme carrier transfer mechanism, *Mol. Catal.*, 2018, **458**, 33–42.

37 M. X. Chen, Y. Z. Dai, J. Guo, H. T. Yang, D. N. Liu and Y. L. Zhai, Solvothermal synthesis of biochar@$ZnFe_2O_4$/BiOBr Z-scheme heterojunction for efficient photocatalytic ciprofloxacin degradation under visible light, *Appl. Surf. Sci.*, 2019, **493**, 1361–1367.

38 M. Zhang, J. L. Gong, G. M. Zeng, P. Zhang, B. Song, W. C. Cao, H. Y. Liu and S. Y. Huan, Enhanced degradation performance of organic dyes removal by bismuth vanadate-reduced graphene oxide composites under visible light radiation, *Colloids Surf., A*, 2018, **559**, 169–183.

39 M. Rafique, M. Hamza, M. B. Tahir, S. Muhammad and A. G. Sehemi, Facile hydrothermal synthesis of highly efficient and visible light-driven Ni-doped V_2O_5 photocatalyst for degradation of Rhodamine B dye, *J. Mater. Sci.: Mater. Electron.*, 2020, **31**, 12913–12925.

40 T. Xie, T. Liao, C. Liu and L. Xu, Synthesis of multifunctional photocatalyst vanadium oxide/activated carbon via in situ utilization of stone coal ore, *Ceram. Int.*, 2018, **45**(4), 4934–4944.

41 S. V. P. Vattikuti, P. A. K. Reddy, P. C. Nagajyothi, J. Shim and C. Byon, Hydrothermally synthesized $Na_2Ti_3O_7$ nanotube-V_2O_5 heterostructures with improved visible photocatalytic degradation and hydrogen evolution-its photocorrosion suppression, *J. Alloys Compd.*, 2018, **740**, 574–586.

42 S. Kundu, B. Satpati, T. Kar and S. K. Pradhan, Microstructure characterization of hydrothermally synthesized PANI/$V_2O_5 \cdot nH_2O$ heterojunction photocatalyst for visible light induced photodegradation of organic pollutants and non-absorbing colorless molecules, *J. Hazard. Mater.*, 2017, **339**, 161–173.

43 X. Kong, L. Li, Z. Guo, C. Zeng, J. Huang and C. Li, Soft chemical in situ synthesis and photocatalytic performance of 1D Ag/AgCl/V_2O_5 hetero-nanostructures, *Mater. Lett.*, 2016, **183**, 215–218.

44 R. Suresh, K. Giribabu, L. Vijayalakshmi and A. Stephen, Visible Light Photocatalytic Property of Zn doped V_2O_5 Nanoparticles, *AIP Conf. Proc.*, 2012, **1447**, 351–352.

45 S. Liu, K. Yin, W. Ren, B. Cheng and J. Yu, Preparation of narrow band gap V_2O_5/TiO_2 composite films by micro-arc oxidation, *Int. J. Miner., Metall. Mater.*, 2012, **22**, 1045–1051.

46 G. F. Liao, J. S. Fang, Q. Li, S. H. Li, Z. S. Xu and B. Z. Fang, Ag-Based nanocomposites: synthesis and applications in catalysis, *Nanoscale*, 2019, **11**, 7062–7096.

47 W. W. Zhong, S. J. Shen, S. S. Feng, Z. P. Lin, Z. P. Wang and B. Z. Fang, Facile fabrication of alveolate $Cu_{2-X}Se$ microsheets as a new visible-light photocatalyst for discoloration of Rhodamine B, *CrystEngComm*, 2018, **20**, 7851–7856.